Monte Carlo Simulation of Scattering from a Layer of Vertical Cylinders

K. Sarabandi, *Senior Member, IEEE*, P. F. Polatin and F. T. Ulaby, *Fellow, IEEE*

Abstract— **The problem of electromagnetic scattering by a collection of randomly distributed vertical cylinders over a half-space dielectric is considered in this paper. The solution to this problem is sought in two ways. In the first approach, a Monte Carlo simulation is used which takes into account scattering terms up to second order. Closed-form expressions for the second-order scattering terms are derived for cylinders that are in the near field of each other. The second approach is based on the radiative transfer (RT) equations which are solved by an iterative method up to and including the second-order terms. Radar backscatter measurements were conducted at X band for a collection of metallic cylinders over a conducting ground plane and these results were compared with the Monte Carlo and radiative transfer solutions. The data were acquired polarimetrically from 144 independent spots of the cylinder layer at incidence angles ranging from 20° to 60°.**

The Monte Carlo simulation agrees well with the measured data and is used to check the validity of the results based on the RT theory for a medium with large particles. It is shown that both the phase function computed for the cylinders and the extinction matrix of the layer are overestimated in the RT solution because the correlation distance for the field inside the medium is smaller than the overall length of the cylinders.

I. Introduction

THE earth's vegetation cover plays an important role in the global carbon cycle, which in turn influences global climatic changes. Advances in the technology of synthetic aperture radars have suggested the possibility of utilizing radar backscatter data to retrieve the biophysical parameters of vegetation canopies. In recent years considerable effort has been devoted to the development of theoretical scattering models for forest canopies. A forest canopy is considered to be an inhomogeneous medium composed of scattering elements with different sizes, shapes, and geometries [23], [24], [5], [4]. Except for the analytical wave approach [18], [3], [8], which accounts for the particles in the medium through a fluctuating permittivity function, all existing methods account for the particles through the single scattering properties of the individual scatterers [9], [17], [7], [19]. The analytical wave approach is appropriate for media where the ratio of the fluctuating dielectric to the mean dielectric is small. Therefore, at microwave and millimeter-wave frequencies, where the dielectric constants of leaves and branches are much larger than that of air, the analytical wave approach may not be appropriate. The solution of the scattering problem for a canopy consisting of discrete scatterers can be tackled in two ways: (1) the field approach [9] and (2) the intensity approach [24]. Because of the complexity of the methodology the solution based on the field approach is limited to sparse particle distributions. The intensity approach or the radiative transfer method (RT) is very general, widely used, mathematically convenient, and therefore useful for inversion algorithms.

In applying RT to a forest medium, some basic conditions necessary to the validity of the method have been overlooked. This model is based on the single scattering properties of the particles in the medium; i.e., it is assumed that particles are in the far field of each other and are illuminated, locally, by plane waves. A tree canopy usually contains particles, such as trunks and branches, which are much larger in dimension than a wavelength; therefore, the far-field condition is not satisfied. Moreover, since these large particles are embedded in a random medium, the magnitude and phase of the field distribution illuminating the particles are nonuniform; thus, the plane wave illumination condition is violated.

It is the purpose of this paper to demonstrate the shortcomings of the radiative transfer technique for a medium containing particles large compared with the wavelength of radiation in the medium. The trunk layer of a forest canopy consisting of vertical dielectric cylinders over a dielectric surface is considered. A Monte Carlo simulation of the scattering problem, which includes multiple scattering up to second order, is developed to provide a realistic solution for comparison. The second-order scattering term in this solution allows the long cylinders to be in the near field of each other. The validity of the Monte Carlo simulation is verfied with experimental backscatter data collected from a random distribution of metallic cylinders over a perfectly conducting ground plane.

II. Scattering from Two Adjacent Cylinders at Oblique Incidence

Exact analytical solutions to the electromagnetic scattering problem exist for only a very limited number of geometries, including infinite cylinders. It has been shown that for cylinders that are very long relative to the wavelength, an approximate solution can be obtained based on the solution for the infinite length case provided $d/L \ll 1$, where d and L are the cylinder diameter and the length, respectively [25], [6]. Although more accurate solutions for the finite-length cylinder can be obtained using numerical techniques, the solutions obtained in this way are not desirable since they become very inefficient when the dimensions of the cylinder are large compared with the

Manuscript received June 23, 1992; revised December 7, 1992.

The authors are with the Radiation Laboratory, Department of Electrical Engineering and Computer Science, University of Michigan, Ann Arbor, MI 48109-2122.

IEEE Log Number 9208148.

wavelength. Similarly, for two finite-length cylinders adjacent to one another, an exact solution does not exist and numerical solutions are even more inefficient. In this paper we resort to an approximate iterative scattering solution. We assume that the cylinders are much longer than the excitation wavelength and that they are mutually in the near field with respect to their longitudinal dimensions but are in the far field with respect to their diameters.

The approach taken is to find the scattered field from the first cylinder as an isolated body given a primary plane-wave excitation. The response of a second cylinder to the cylindrical-wave excitation from the first cylinder is then found. The effect of the second cylinder on the first is obtained by reciprocity. In this way an approximate analytical solution may be obtained which accounts for multiple scattering to second order. In principle, this procedure can be continued to any desired order of approximation; however, a price is paid in terms of the complexity of the final solution.

By invoking the field equivalence principle, the cylinders can be replaced by equivalent electric and magnetic surface current densities given by

$$\mathbf{J}_e(\phi, z) = \hat{n} \times \mathbf{H} \tag{1}$$

and

$$\mathbf{J}_m(\phi, z) = -\hat{n} \times \mathbf{E} \tag{2}$$

where $\mathbf{E}$ and $\mathbf{H}$ are the total electric and magnetic fields on the cylinder surface and $\hat{n}$ is the outward surface normal. If the surface currents are known, the scattered electric field may be obtained from

$$\mathbf{E}^s(\mathbf{r}) = \nabla \times \nabla \times \mathbf{\Pi}_e(\mathbf{r}) + ik_0 Z_0 \nabla \times \mathbf{\Pi}_m(\mathbf{r}), \tag{3}$$

where $\mathbf{\Pi}_e$ and $\mathbf{\Pi}_m$ are the electric and magnetic Hertz vector potentials respectively. The electric Hertz vector potential is given by

$$\mathbf{\Pi}_e = \frac{iZ_0}{4\pi k_0} \int_S \mathbf{J}_e(\mathbf{r}') \frac{e^{ik_0|\mathbf{r}-\mathbf{r}'|}}{|\mathbf{r}-\mathbf{r}'|} dS'. \tag{4}$$

In this paper the $e^{-i\omega t}$ time convention has been assumed and will be suppressed throughout. The magnetic Hertz vector potential has a similar form with Z_0 replaced by Z_0^{-1} and $\mathbf{J}_e$ replaced by $\mathbf{J}_m$.

The surface currents on a long cylinder are approximated by the surface currents on a corresponding infinite cylinder of the same diameter. These surface currents have also been separated into a traveling wave component along the cylinder's axial direction and a circumferential component [14]. The expressions for these currents are given by

$$\mathbf{J}_{\substack{e \\ m}}(\phi, z) = \mathbf{J}_{\substack{e \\ m}}(\phi) e^{-ik_0 \cos\beta z}.$$

The circumferential components of surface current density are

$$\mathbf{J}_e(\phi) = Y_0(\sin\phi\hat{x} - \cos\phi\hat{y})$$

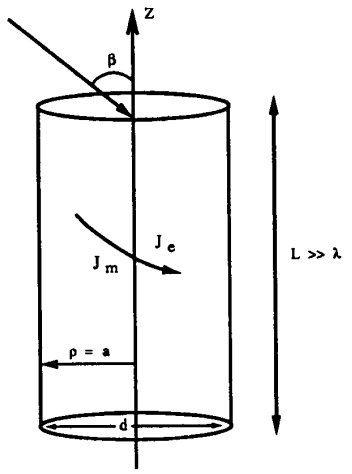

Fig. 1. Geometry of a long cylinder with equivalent electric and magnetic currents on the surface.

$$\sum_{m=-\infty}^{+\infty} (-i)^m \{h_z J_m(x_0) + B_m H_m^{(1)}(x_0)\} e^{im\phi} - \frac{Y_0}{ik_0 \sin^2\beta}\hat{z} \cdot \sum_{m=-\infty}^{+\infty} (-i)^m \left\{k_0 \sin\beta \left[e_z J_m'(x_0) + A_m H_m^{(1)'}(x_0)\right] + \frac{im\cos\beta}{\rho_1}\left[h_z J_m(x_0) + B_m H_m^{(1)}(x_0)\right]\right\} e^{im\phi} \tag{5}$$

and

$$\mathbf{J}_m(\phi) = -(\sin\phi\hat{x} - \cos\phi\hat{y}) \sum_{m=-\infty}^{+\infty} (-i)^m \{e_z J_m(x_0) + A_m H_m^{(1)}(x_0)\} e^{im\phi} - \frac{Y_0}{ik_0 \sin^2\beta}\hat{z} \sum_{m=-\infty}^{+\infty} (-i)^m \left\{k_0 \sin\beta \left[h_z J_m'(x_0) + B_m H_m^{(1)'}(x_0)\right] - \frac{im\cos\beta}{\rho_1}\left[e_z J_m(x_0) + A_m H_m^{(1)'}(x_0)\right]\right\} e^{im\phi}, \tag{6}$$

where β is the angle of incidence (see Fig. 1) and $x_0 = k_0 a \sin\beta$, with a being the cylinder radius.

In this case, the expression for the electric Hertz vector potential simplifies to

$$\mathbf{\Pi}_e = \frac{iZ_0}{4\pi k_0} \int_0^{2\pi} \mathbf{J}_e(\phi') \int_0^L \frac{e^{ik_0(|\mathbf{r}-\mathbf{r}'| - \cos\beta z')}}{|\mathbf{r}-\mathbf{r}'|} a dz' d\phi'. \tag{7}$$

If the observation point (x, y) satisfies the condition $k_0 \sin\beta\sqrt{x^2+y^2} \gg 1$, the z' integration can be evaluated using the stationary phase approximation. The condition for the stationary phase is

$$\frac{d}{dz'}(|\mathbf{r}-\mathbf{r}'| - \cos\beta z') = 0,$$

which, in this case, implies

$$z'_{SP} = z + \frac{\cos\beta\sqrt{(x-x')^2+(y-y')^2}}{\sin\beta}$$

and the stationary point is on the surface of a cone of half-angle β which contains the observation point. Performing the integration with respect to z' yields

$$\int_0^L \frac{e^{ik_0(|\mathbf{r}-\mathbf{r}'|-\cos\beta z')}}{|\mathbf{r}-\mathbf{r}'|}dz' = \sqrt{\frac{2\pi}{k_0\sin\beta\tilde{\rho}}}e^{i(k_0\sin\beta\tilde{\rho}-\pi/4)} \times e^{-ik_0\cos\beta z}e^{-ik_0 a\sin\beta\cos(\phi'-\tilde{\phi})}. \tag{8}$$

Applying the far-field condition in the $x-y$ plane, the curl operator reduces to $\nabla\times \approx ik_0\hat{k}_s\times$, where

$$\hat{k}_s = \sin\beta(\cos\tilde{\phi}\hat{x}+\sin\tilde{\phi}\hat{y})-\cos\beta\hat{z}$$

and the expression for the scattered field simplifies to

$$\mathbf{E}^s = k_0^2(\hat{k}_s\times\hat{k}_s\times\mathbf{\Pi}_e - Z_0\hat{k}_s\times\mathbf{\Pi}_m). \tag{9}$$

Substituting (5) and (8) into (7) the remaining integration with respect to ϕ' is accomplished with the aid of the following integral relations [22]:

$$\int_0^{2\pi} e^{-ik_0\rho_1 B\cos(\phi'-\tilde{\phi})}e^{im\phi'} = 2\pi(-i)^m J_m(y_0)e^{im\tilde{\phi}}$$

$$\int_0^{2\pi}\begin{Bmatrix}\cos\phi'\\ \sin\phi'\end{Bmatrix}e^{-ik_0\rho_1 B\cos(\phi'-\tilde{\phi})}e^{im\phi'} = 2\pi(-i)^m\left[i\begin{Bmatrix}\cos\tilde{\phi}\\ \sin\tilde{\phi}\end{Bmatrix}J'_m(y_0)+\begin{Bmatrix}\sin\tilde{\phi}\\ -\cos\tilde{\phi}\end{Bmatrix}\frac{m}{y_0}J_m(y_0)\right]e^{im\tilde{\phi}}$$

with $B = \{[(\hat{k}_s-\hat{k}_i)\cdot\hat{x}]^2+[(\hat{k}_s-\hat{k}_i)\cdot\hat{y}]^2\}^{1/2}$ and $y_0 = k_0 aB$. The definitions of $\tilde{\phi}$ and $\tilde{\rho}$ are given in Fig. 2. After lengthy algebraic manipulations the scattered field from the first cylinder is found to be

$$\mathbf{E}_1^s = \mathbf{F}(\tilde{\phi})H_0^{(1)}(k_0\sin\beta\tilde{\rho})e^{-ik_0 z\cos\beta}, \tag{10}$$

in which

$$\mathbf{F}(\tilde{\phi}) = \frac{-1}{\sin^2\beta}\sum_{m=-\infty}^{+\infty}(-1)^m \times[A_m(\hat{k}_s\times\hat{k}_s\times\hat{z})+B_m(\hat{k}_s\times\hat{z})]e^{im\tilde{\phi}}. \tag{11}$$

The coefficients A_m and B_m are given in terms of components that are TE_z and TM_z:

$$A_m = C_m^{\mathrm{TM}}\mathbf{E}^i\cdot\hat{z}+i\bar{C}_m\mathbf{H}^i\cdot\hat{z}$$
$$B_m = C_m^{\mathrm{TE}}\mathbf{H}^i\cdot\hat{z}-i\bar{C}_m\mathbf{E}^i\cdot\hat{z} \tag{12}$$

and the expressions for C_m^{TE}, C_m^{TM} and $\bar{C}_m$ are given in [13].

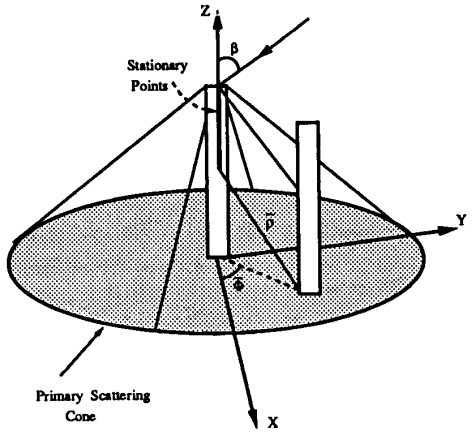

Fig. 2. Geometry of dual-cylinder configuration and second-order interaction.

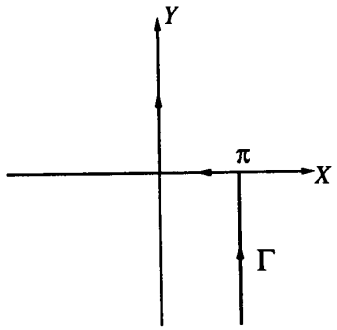

Fig. 3. Integration contour in complexγ plane.

A. Second-Order Interaction

Referring to (10), the Hankel function of the scattered cylindrical wave may now be expressed as a continuous spectrum of plane waves:

$$H_0^{(1)}(k_0\sin\beta\tilde{\rho}) = \frac{1}{\pi}\int_\Gamma e^{ik_0\sin\beta(\cos\gamma x+\sin\gamma|y|)}d\gamma, \tag{13}$$

where the contour of integration Γ is shown in Fig. 3.

Each scattered wave from the second cylinder as a result of the plane wave spectrum excitation from the first cylinder can be summed by superposition to obtain the total scattered field from the second cylinder. With regard to the stationary phase approximation, only a subset of stationary points on the surface of the first cylinder acts as a source of illumination for the second cylinder. Stationary points not located on the cylinder surface give no contribution to the secondary scattered wave. We have assumed that since the length L of the first cylinder is much greater than the excitation wavelength, most of the primary scattered fields are contained in the forward scattering cone. We now also assume that $(L-\tilde{\rho}\cos\beta)\gg\lambda_0$, so the scattered field from each incident plane wave in the expansion is confined to the forward scattering cone. The total

scattered field from the second cylinder is then given by

$$\mathbf{E}_2^s = \frac{1}{\pi}\int_\Gamma \mathbf{e}_2^s(\gamma)d\gamma, \tag{14}$$

in which the direction of each incident plane wave is

$$\hat{k}_i = \sin\beta(\cos\gamma\hat{x} + \sin\gamma\hat{y}) - \cos\beta\hat{z}$$

and the contour Γ has been described previously.

Again each individual secondary scattered field can be described in terms of TE_z and TM_z components. Then, in the far zone, these fields may be written as

$$\mathbf{e}_2^s(\gamma) = e^{ik_0\hat{k}_i\cdot\vec{r}_2}\frac{e^{ik_0R}}{R}\left[\frac{-i(L-\tilde{\rho}\cot\beta)}{\pi\sin^2\beta}\right]\frac{\sin V}{V}$$
$$\sum_{m=-\infty}^{+\infty}(-1)^m[A'_m(\hat{k}_s\times\hat{k}_s\times\hat{z}) + B'_m(\hat{k}_s\times\hat{z})], \tag{15}$$

with

$$\vec{r}_2 = \tilde{\rho}\cos\tilde{\phi}\hat{x} + \tilde{\rho}\sin\tilde{\phi}\hat{y} + \left(\frac{L-\tilde{\rho}\cot\beta}{2}\right)\hat{z}$$
$$R = r - \hat{k}_s\cdot\vec{r}_2$$
$$V = \frac{k_0(L-\tilde{\rho}\cot\beta)}{2}(\cos\beta_s - \cos\beta)$$
$$\hat{k}_s = \sin\beta_s(\cos\phi_s\hat{x} + \sin\phi_s\hat{y}) - \cos\phi_s\hat{z} \tag{16}$$

and

$$A'_m = \sum_{n=-\infty}^{+\infty}(-1)^n[A_nC_m^{TM} + iB_n\bar{C}_m]e^{in\tilde{\phi}}$$
$$B'_m = \sum_{n=-\infty}^{+\infty}(-1)^n[B_nC_m^{TE} - iA_n\bar{C}_m]e^{in\tilde{\phi}}, \tag{17}$$

where A_n and B_n are as given in (12) and $\cos\beta_s = \hat{k}_s\cdot\hat{z}$.

Substituting (15) into (14) and using the change of variable $\gamma' = \tilde{\phi}+\gamma$, an analytical expression for the secondary scattered wave in the far zone is found to be

$$\mathbf{E}_2^s = \frac{e^{ik_0r}}{r}e^{-ik_0\sin\beta\tilde{\rho}\cos(\phi_s-\tilde{\phi})}\left[\frac{-i(L-\tilde{\rho}\cot\beta)}{\pi\sin^2\beta}\right]\frac{\sin V}{V}e^{iV}$$
$$\sum_{m=-\infty}^{+\infty}(-1)^m[A'_m(\hat{k}_s\times\hat{k}_s\times\hat{z}) + B'_m(\hat{k}_s\times\hat{z})]$$
$$H_m^{(1)}(k_0\sin\beta\tilde{\rho})e^{im(\phi_s-\tilde{\phi})}. \tag{18}$$

B. Effect of Ground Plane

The next step toward obtaining the scattered field from a layer of cylinders above a dielectric half-space is to consider the problem of two adjacent cylinders above a dielectric half-space. The level of difficulty involved in obtaining a solution for this problem is greater than for the previous problem owing to the complexity of the Green function in this case. The Green function for this type of problem has an integral form, and obtaining an analytical expression for this solution is impossible. A numerical solution with a great deal of complexity can be obtained by applying exact image theory [10], [15]. Here again we are approximating the form of the Green function by assuming that the image of the source point is a source point located on the opposite side of the half-space interface (mirror-image point) and modified by the appropriate reflection coefficient. This approximation is very accurate when the source or observation point is not close to the interface and becomes exact when the ground plane is perfectly conducting. To apply this simple approximation we decompose the incident and scattered fields into TE and TM components. The effect of the ground plane will then be accounted for by modifying these field components by their appropriate reflection coefficients.

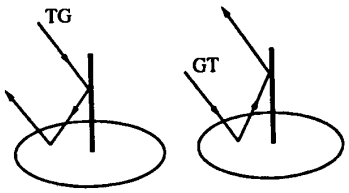

Fig. 4. First-order interactions of a cylinder with the ground plane.

The first-order interactions are shown in Fig. 4. In the trunk–ground (TG) interaction, the primary scattered field is modified by interaction with the ground plane. The reflected field for this interaction is obtained by multiplying the TE and TM components of (10) by the appropriate reflection coefficient to produce

$$\mathbf{E}_{tg}^s = \frac{e^{ik_0r}}{r}e^{-ik_0\frac{L}{2}(\cos\beta_s-\cos\beta)}\left[\frac{-iL}{\pi\sin^2\beta}\right]\frac{\sin U}{U}$$
$$\sum_{m=-\infty}^{+\infty}(-1)^m[A_mR_\parallel(\hat{k}_s\times\hat{k}_s\times\hat{z}) + B_mR_\perp(\hat{k}_s\times\hat{z})]e^{im\phi_s}, \tag{19}$$

where A_m and B_m are defined in (12), β_s and ϕ_s represent the direction of the scattered wave, and $U = k_0L(\cos\beta_s - \cos\beta)/2$. The other type of first-order interaction is ground–trunk (GT) and consists of modification of the primary scattered wave from a cylinder by the ground plane reflection coefficients. It is found in the same manner as above and is given by

$$\mathbf{E}_{gt}^s = \frac{e^{ik_0r}}{r}e^{-ik_0\frac{L}{2}(\cos\beta_s-\cos\beta)}\left[\frac{-iL}{\pi\sin^2\beta}\right]\frac{\sin U}{U}$$
$$\sum_{m=-\infty}^{+\infty}(-1)^m[A_m^r(\hat{k}_s\times\hat{k}_s\times\hat{z}) + B_m^r(\hat{k}_s\times\hat{z})]e^{im\phi_s}, \tag{20}$$

where

$$A_m^r = C_m^{TM}R_\parallel\,\mathbf{E}^i\cdot\hat{z} + i\bar{C}_m\,R_\perp\,\mathbf{H}^i\cdot\hat{z}$$
$$B_m^r = C_m^{TE}R_\perp\,\mathbf{H}^i\cdot\hat{z} - i\bar{C}_m\,R_\parallel\,\mathbf{E}^i\cdot\hat{z}. \tag{21}$$

The second-order interactions are trunk–trunk–ground (TTG), trunk–ground–trunk (TGT), and ground–trunk–trunk (GTT). The mechanisms are illustrated in Fig. 5. The TTG interaction may be obtained simply by taking the two cylinder scattering equation (18) and modifying the

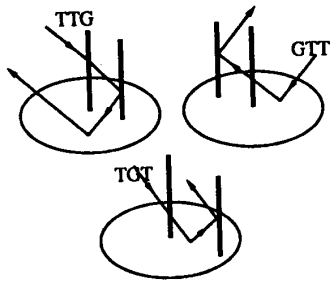

Fig. 5. Second-order interactions of two cylinders with the ground plane.

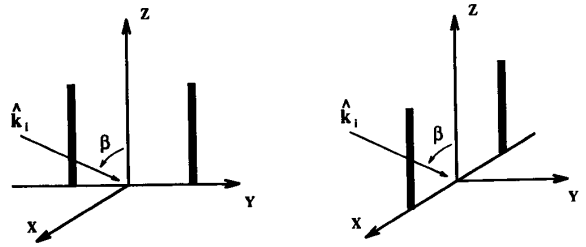

BROADSIDE CONFIGURATION ENDFIRE CONFIGURATION

Fig. 6. Broadside and end-fire cylinder configurations. Wave incident in $X-Z$ plane with incidence angle β.

appropriate components by their respective ground plane reflection coefficients to obtain

$$\mathbf{E}^s_{ttg} = \frac{e^{ik_0 r}}{r} e^{-ik_0 \sin\beta\tilde{\rho}\cos(\phi_s-\tilde{\phi})} \left[\frac{-i(L-\tilde{\rho}\cot\beta)}{\pi \sin^2\beta}\right] \frac{\sin V}{V} e^{iV} \sum_{m=-\infty}^{+\infty} (i)^m [A'_m R_{\|} (\hat{k}_s \times \hat{k}_s \times \hat{z}) + B'_m R_{\perp} (\hat{k}_s \times \hat{z})] H_m^{(1)}(k_0 \sin\beta\tilde{\rho}) e^{im(\phi_s-\tilde{\phi})}, \quad (22)$$

where A'_m and B'_m are given in (17) and V in (16).

The TGT scattered wave is obtained by exciting a single cylinder with the expanded field of the TG interaction over its lower $\tilde{\rho}\cot\beta$ portion in a manner completely analagous to what has already been done. The result is

$$\mathbf{E}^s_{tgt} = \frac{e^{ik_0 r}}{r} e^{-ik_0 \sin\beta\tilde{\rho}\cos(\phi_s-\tilde{\phi})} \left[\frac{-i\tilde{\rho}\cot\beta}{\pi \sin^2\beta}\right] \frac{\sin V'}{V'} e^{iV'} \sum_{m=-\infty}^{+\infty} (i)^m [A''_m (\hat{k}_s \times \hat{k}_s \times \hat{z}) + B''_m (\hat{k}_s \times \hat{z})] H_m^{(1)}(k_0 \sin\beta\tilde{\rho}) e^{im(\phi_s-\tilde{\phi})} \quad (23)$$

where

$$V' = \frac{k_0\tilde{\rho}\cot\beta}{2} (\cos\beta_s - \cos\beta) \quad (24)$$

and

$$A''_m = \sum_{n=-\infty}^{+\infty} (-1)^n [A_n R_{\|} C_m^{TM} + iB_n R_{\perp} \bar{C}_m] e^{in\tilde{\phi}}$$

$$B''_m = \sum_{n=-\infty}^{+\infty} (-1)^n [B_n R_{\perp} C_m^{TE} - iA_n R_{\|} \bar{C}_m] e^{in\tilde{\phi}}. \quad (25)$$

Finally, the GTT field is obtained using the same approach:

$$\mathbf{E}^s_{gtt} = \frac{e^{ik_0 r}}{r} e^{-ik_0 \sin\beta\tilde{\rho}\cos(\phi_s-\tilde{\phi})} \left[\frac{-i(L-\tilde{\rho}\cot\beta)}{\pi \sin^2\beta}\right] \frac{\sin V}{V} e^{-iW} \sum_{m=-\infty}^{+\infty} (i)^m [A'''_m (\hat{k}_s \times \hat{k}_s \times \hat{z}) + B'''_m (\hat{k}_s \times \hat{z})] H_m^{(1)}(k_0 \sin\beta\tilde{\rho}) e^{im(\phi_s-\tilde{\phi})}, \quad (26)$$

with

$$W = \frac{k_0(L+\tilde{\rho}\cot\beta)}{2} (\cos\beta_s - \cos\beta) \quad (27)$$

and

$$A'''_m = \sum_{n=-\infty}^{+\infty} (-1)^n [A_n^r C_m^{TM} + iB_n^r \bar{C}_m] e^{in\tilde{\phi}}$$

$$B'''_m = \sum_{n=-\infty}^{+\infty} (-1)^n [B_n^r C_m^{TE} - iA_n^r \bar{C}_m] e^{in\tilde{\phi}}, \quad (28)$$

where A_n^r and B_n^r are as given in (21) and V as in (16).

The total far-zone scattered field to second order is then the sum of the terms given above:

$$\mathbf{E}^s = \mathbf{E}^s_{tg} + \mathbf{E}^s_{gt} + \mathbf{E}^s_{ttg} + \mathbf{E}^s_{tgt} + \mathbf{E}^s_{gtt}. \quad (29)$$

The corresponding scattering matrix elements for each term are given in the appendix.

Measurements were performed at X band (9.5 GHz) using a polarimetric scatterometer to validate the expressions derived for two adjacent cylinders above a ground plane. A pair of metallic rods 18 cm in length and 0.56 cm in diameter were arranged above a large metallic ground plane with various separations and orientations relative to the illuminating beam. The cylinder positions relative to the incident wave direction and the incidence angle for the cases of broadside and end-fire illumination are shown in Fig. 6. Fig. 7 compares the first- and second-order theoretical predictions of the radar cross section for the two cylinders with the measured values in the case of 2 cm separation and broadside configuration. Figs. 8 and 9 compare the measured and predicted values of RCS for a separation of 4 cm in the end-fire configuration. The experimental data agree well with the second-order results. The first-order approximation does not provide an adequate estimation of RCS for cylinder separations within this general range. It is seen that the first- and second-order results do not differ significantly for σ_{hh} because the cylinders are relatively thin and therefore the horizontally polarized incident wave is only weakly scattered. Discrepancies between the measured and computed values of RCS are observed at the lower angles of incidence because of scattering by the cylinder end caps, which is ignored in the theoretical formulation.

III. Monte Carlo Simulation

Having validated the expressions derived for adjacent pairs of cylinders, we now attempt to obtain the scattering properties

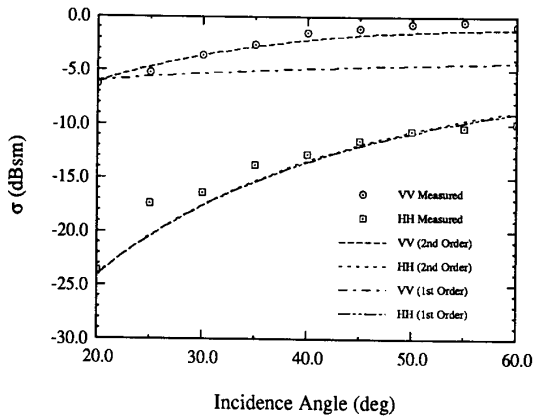

Fig. 7. RCS of two rods broadside on metal plate at 9.5 GHz: 2 cm separation.

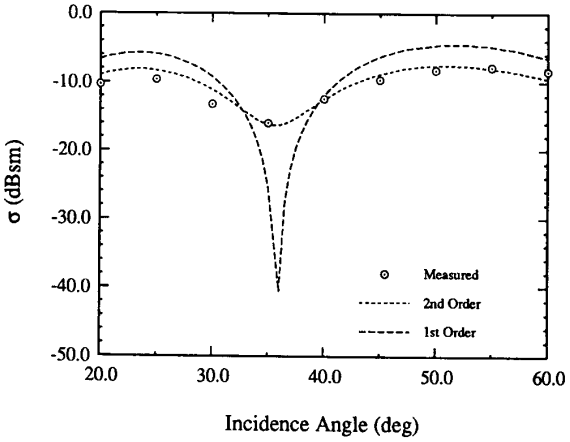

Fig. 8. RCS of two rods end-fire on metal plate (VV-pol.) at 9.5 GHz: 4 cm separation.

of random collections of such cylinders above a ground plane. For a given arrangement consisting of many cylinders, the solution of the scattering problem can be obtained to second order by computing the single and pairwise interactions for every cylinder in the ensemble. The statistical properties of a random medium made up of such scatterers are simulated by application of the Monte Carlo method.

The principle of the Monte Carlo simulation based on the second-order algorithm is as follows:

1. An ensemble of randomly positioned cylinders is generated using a random number generator. In this case the cylinder positions are uniformly distributed within a circular area. The number of cylinders used is dependent on the specified number per unit area and the area of the circular region.
2. The scattering is computed for all cylinders and between all pairs of cylinders within the ensemble up to second order.
3. The ensemble is rerandomized and the scattering recomputed as discussed above. The number of independent samples is chosen so as to make the variance as small as possible within limits depending on the computing time. For the cases analyzed in this article the sample number is greater than 100.
4. The values of the scattering coefficients $(\sigma^o_{vv}, \sigma^o_{hh})$ are found from the ensemble average. The same is true for the copolarized phase difference ζ, and the degree of copolarized phase correlation α [16].

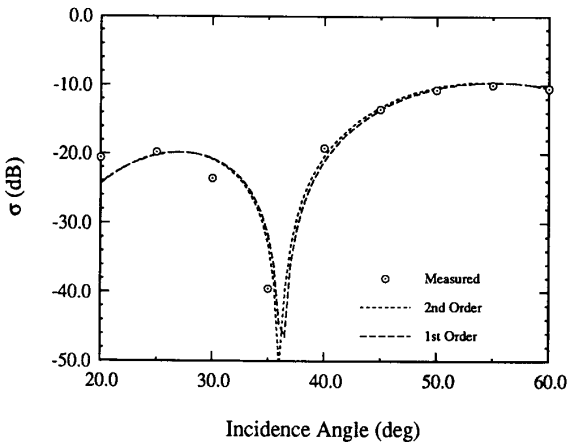

Fig. 9. RCS of two rods end-fire on metal plate (HH-pol.) at 9.5 GHz: 4 cm separation.

Measurements of radar backscatter were also made on random collections of cylinders distributed within a circular area as described for the Monte Carlo simulation as an experimental verification of the simulation. Identical metal cylinders 18 cm in length and 0.56 cm in diameter were uniformly distributed within a 60 cm diameter circular area with densities of 70, 100, 140, and 180 per square meter. Radar measurements were made with an X-band scatterometer at incidence (elevation) angles relative to the vertical axis ranging from 20° to 60° in 5° increments. Samples were generated by arranging the cylinders on four separate thin plastic disks with independently generated holes for supporting the cylinders. The edge diffraction contribution of the ground plane to the overall RCS of the cylinder/ground plane system was removed by measuring the ground plane without the cylinders present and coherently subtracting this measurement from that of the combined system. Each disk was rotated in 10° increments to create distinct aspects for the radar. In this way 144 independent samples were generated at each density level. The final measurements were tested for correlation to ensure that the sampling was independent. The experimental setup is illustrated in Fig. 10.

The correspondence of the simulation to the measurements of σ^o as a function of incidence angle for the case of 70 cylinders per square meter is shown in Fig. 11. The first- and second-order Monte Carlo simulations agree very well with the experimental data. Apparently, for the type of random medium considered in this study, the effect of multiple scattering between cylinders is averaged out as far as the magnitude of the radar backscatter is concerned. This

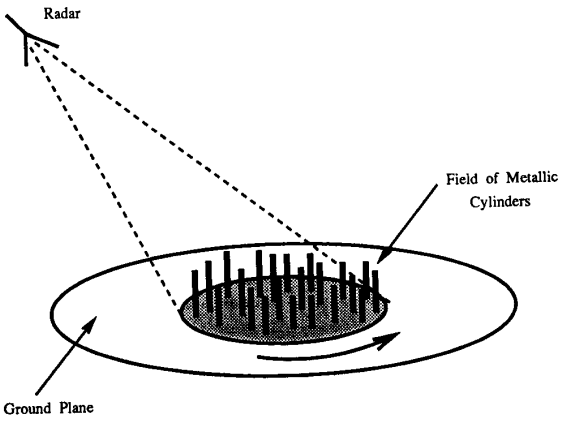

Fig. 10. Measurement of metallic cylinder field.

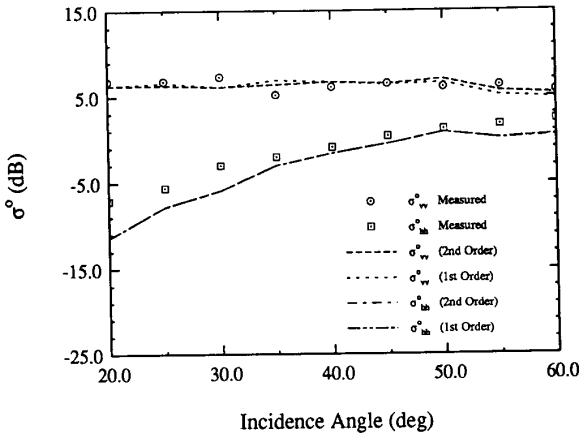

Fig. 11. Backscattering coefficient of a layer of uniformly distributed metal cylinders above perfectly conducting ground plane (density = 70 cyls/m^2).

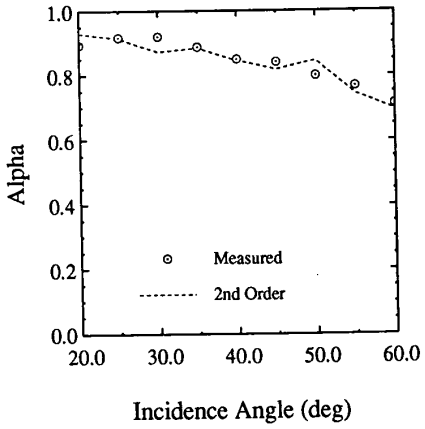

Fig. 12. Copolarized degree of correlation for a layer of uniformly distributed metal cylinders above perfectly conducting ground plane (density =70 cyls/m^2).

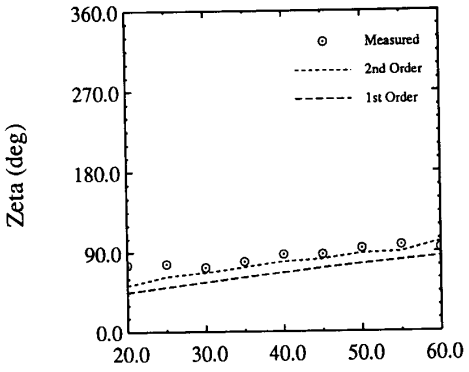

Fig. 13. Copolarized phase difference for a layer of uniformly distributed metallic cylinders above a perfectly conducting ground plane (density =70 cyls/m^2).

is why the first-order results agree well with the copolarized radar cross section measurements. Figs. 12 and 13 illustrate the agreement between measurement and simulation for the copolarized phase statistics. It should be noted that for both α and ζ, inclusion of the second-order terms provides the correct phase statistics while the first-order scattering theory is significantly in error. Since α is a sensitive function of the degree of multiple scattering within a medium, first-order theory incorrectly predicts a value of unity independent of the number density of particles.

IV. Comparison with Radiative Transfer

In the last decade or so the radiative transfer approach has been widely used in modeling electromagnetic scattering from vegetation media [4], [24], [11], [12], [21], [5]. It is based on coupled differential equations describing the transport of energy within a medium and is therefore an incoherent (or intensity based) technique. The vector radiative transfer equations take into account the individual scattering properties of the vegetation canopy components through a phase matrix which relates the incident to scattered intensities as a function of the wave directions, scatterer geometry, and scatterer composition. The formulation has the advantage of being general, mathematically convenient, and amenable to inversion.

In a medium in which the individual particle scattering albedos are small and the particles are in the far zone with respect to each another, one would expect that there would be little difference between the Monte Carlo simulation results and those of radiative transfer. Because the scattered fields are added coherently in the Monte Carlo simulation, the computed values of σ^o by this method should be 3 dB above those computed by the incoherent addition of power as in radiative transfer theory for reciprocal scattering mechanisms such as GT and TG. The medium described above in the experimental section of this article consists of metallic cylinders that are long compared with the wavelength of radiation in the

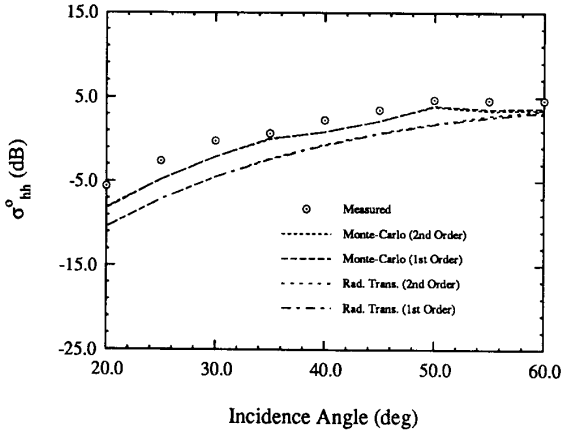

Fig. 14. Comparison of RT model with Monte Carlo simulation and measured data for the cylinder layer with a density of 140 cyls/m^2.

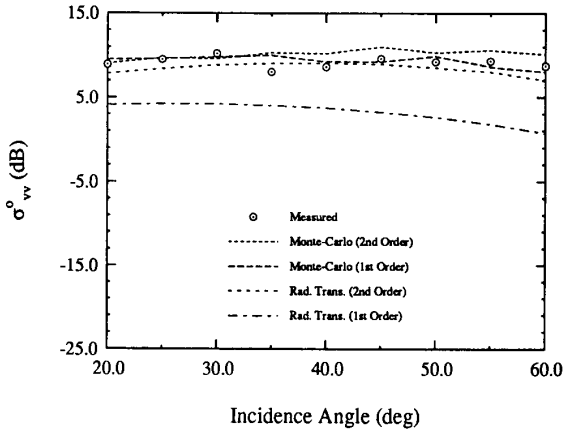

Fig. 15. Comparison of RT model with Monte Carlo simulation and measured data for the cylinder layer with a density of 140 cyls/m^2.

medium; however the diameters of the cylinders are fairly small compared with the excitation wavelength. In this case the far-field condition is satisfied for the wave polarized in the dimension transverse to the cylinder length (HH polarization) and propagation for this polarization is dominated by single scattering. This effect can be seen in Fig. 14, which represents HH polarized backscatter from a fairly dense medium with 140 rods per square meter.

A vertically polarized wave traveling in this cylinder medium encounters particles that are both strong scatterers and in the near field with respect to each other. Because of these conditions the correlation distance for the vertically polarized field in the medium is significantly smaller than the length of a cylinder, yet it is larger than the distance between particles. Therefore the local plane-wave approximation is no longer valid in this regime and, in addition, there is a significant degree of coupling between particles. This would be expected to affect the radiative transfer results in two ways. The phase matrix is utilized by radiative transfer to generate the source functions which drive the coupled set of differential equations for the upward and downward traveling radiation intensities. This phase matrix is linearly dependent on the height squared of the cylinders. If the mechanism of cylinder excitation is not by a plane wave then field decorrelation in the medium can make the effective height of the cylinders to be smaller than their actual length. This means that radiative transfer theory would overestimate the phase matrix of the cylinder medium. On the other hand, the computation of the extinction matrix, which accounts for attenuation of the wave intensity as it propagates in the medium, is linearly dependent on the height of the individual cylinders. If the effective scattering matrix for cylinders in the medium is actually smaller than would be expected on the basis of the local plane-wave approximation, the extinction matrix for the medium would also be smaller than that normally used in radiative transfer. Because extinction is an exponential process it has a large effect on the computation of the VV polarized radar cross section.

Fig. 15 shows that while first- and second-order Monte Carlo simulations agree fairly well with measured data in the computation of σ^o_{vv}, first-order radiative transfer gives an estimate that is significantly low. This is also shown by the fact that the first-order radiative transfer solution becomes worse as the angle of incidence increases, which is consistent with overestimation of the extinction and which more than compensates for overestimation of the phase matrix. Even though second-order radiative transfer provides a solution that is more in harmony with the measured results, it would be expected that if the second-order theory were entirely correct this solution should maintain a level consistently about 3 dB lower than the measurements and Monte Carlo results. In addition, in the light of the trend illustrated, it seems unlikely that the radiative transfer solution will converge to the correct level as successively higher order terms are added since all further contributions to the net scattered intensity are guaranteed to be positive and the second-order result is already too high. It is also to be noted that in all cases evaluated by these authors the first-order Monte Carlo simulation provides an excellent estimate of radar cross section. If the radiative transfer approach is valid under these conditions one would wonder why the first order R.T. theory does not give results consistent with this finding.

The degree of correlation α for the phase distribution PDF is sensitive to multiple scattering effects because it is the multiple scattering that produces phase decorrelation in random media. Fig. 16 shows that the second-order Monte Carlo simulation gives good agreement with experimental measurements, indicating that multiple scattering to second order is significant in the medium. The second-order radiative transfer theory gives an erroneously high degree of copolarized phase decorrelation. This demonstrates the overestimation of the phase matrix previously mentioned. In Fig. 17 both the Monte Carlo simulation and the radiative transfer are in agreement with the measured data. It is evident that the copolarized phase difference is not significantly affected by parameters that reflect the differences between these two methods of modeling the canopy.

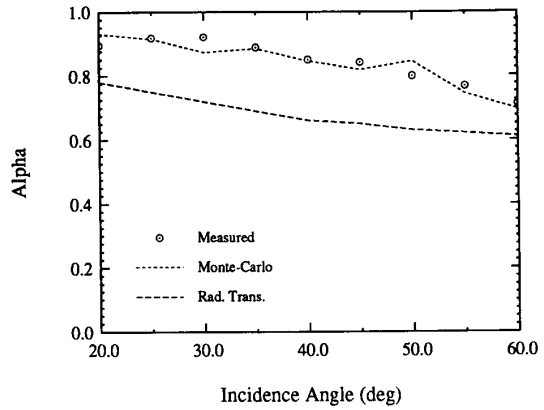

Fig. 16. Comparison of RT model with Monte Carlo simulation and measured data for the cylinder layer with a density of 70 cyls/m^2.

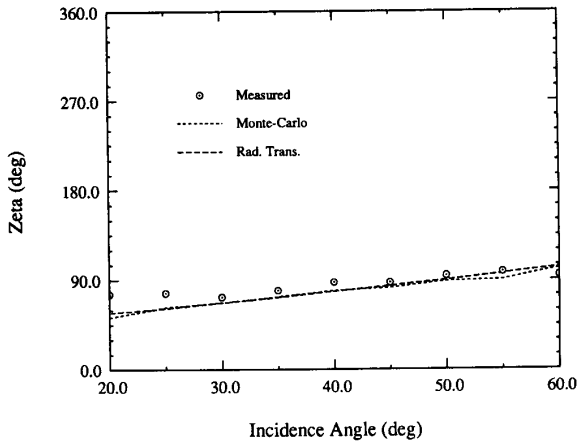

Fig. 17. Comparison of RT model with Monte Carlo simulation and measured data for the cylinder layer with a density of 70 cyls/m^2.

V. Conclusions

In this work, a Monte Carlo scattering model for the trunk layer of a forest canopy has been developed which takes into account scattering effects up to second order. Experimental data have been presented for the purpose of validating the two-cylinder scattering solution, and results of a Monte Carlo simulation based on this solution have also been presented and compared with measured results. First- and second-order radiative transfer model solutions for the same medium have been given and compared with those for the Monte Carlo simulation. It is verified that the radiative transfer model provides incorrect results under conditions such that its basic assumptions are violated. This occurs in media for which the size of the particles is large compared with the wavelength in the medium, which causes the illumination to be nonuniform and/or the medium is dense and therefore the near-field interaction becomes significant. In such cases the phase and extinction matrices used in the radiative transfer model are overestimated and the results will be incorrect.

Appendix
Cylinder Medium Second-Order Scattering Matrix Elements

In this appendix the second-order scattering matrix elements for two adjacent vertical cylinders above a ground plane are given. The elements are obtained by setting $\mathbf{E}^i$ equal to $\hat{v}_i$ and $\hat{h}_i$ and taking the scalar product with $\hat{v}_s$ and $\hat{h}_s$. First defining

$$\Gamma^{\mathrm{TM}} = \sum_{n=-\infty}^{+\infty} (-1)^m C_n^{\mathrm{TM}} e^{in\tilde{\phi}}$$

$$\Gamma^{\mathrm{TE}} = \sum_{n=-\infty}^{+\infty} (-1)^m C_n^{\mathrm{TE}} e^{in\tilde{\phi}}$$

and

$$\bar{\Gamma} = \sum_{n=-\infty}^{+\infty} (-1)^m \bar{C}_n e^{in\tilde{\phi}}$$

the matrix elements for each type of interaction are as shown at the top of the next page.

References

[1] A. K. Fung and H. S. Fung, "Application of the first-order renormalization method to scattering from a vegetated-like half-space," *IEEE Trans. Geosci. Remote Sensing*, vol. 15, pp. 189–195, 1977.

[2] A. K. Fung, "A review of volume scatttering theoies for modeling applications," *Radio Sci.*, vol. 17, pp. 1007–1017, 1982.

[3] A. K. Fung and F. T. Ulaby, "A scatter model for leafy vegetation," *IEEE Trans. Geosci. Remote Sensing*, vol. 16, pp. 281–286, 1978.

[4] M. A Karam and A. K. Fung, "Electromagnetic scattering from a layer of finite length, randomly oriented, dielectric circular cylinders over a rough interface wth application to vegetation," *Int. J. Remote Sensing*, vol. 9, pp. 1109–1134, 1988.

[5] M. A. Karam and A. K. Fung, "Scattering from rendomly oriented circular discs with application to vegetation," *Radio Sci.*, vol. 18, pp. 557–565, 1983.

[6] M. A. Karam and A. K. Fung, "EM scattering from a randomly oriented circular dielectric, finite-length cylinder," in *Proc. Int. Union Radio Sci. Commision F: Wave Propagation and Remote Sensing* (University of New Hampshire, Durham, NH), pp. 4.1.1–4.1.3.

[7] M. A. Karam, A. K. Fung, and Y. M. Antar, "Scattering models for vegetation samples," in *Proc. IEEE Geosci. Remote Sensing Symp.*, vol. 2, 1987, pp. 1013–1018.

[8] R. H. Lang, "Electromagnetic backscattering from a sparse distribution of lossy dielectric scatterers," *Radio Sci.*, vol. 16, pp. 15–30, 1981.

[9] R. H. Lang and J. S. Sidhu, "Electromagnetic backscattering from a layer of vegetation: A discrete approach," *IEEE Trans. Geosci. Remote Sensing*, vol. 21, pp. 62–71, 1983.

[10] I. V. Lindell and E. Alanen, "Exact image theory for the Sommerfeld half-space problem, Part III: General formulation," *IEEE Trans. Antennas Propagat.*, vol. 32, pp. 1027–1032, 1984.

[11] K. C. McDonald, M. C. Dobson, and F. T. Ulaby, "Using MIMICS to model L-band multi-angle and multi-temporal backscatter from a walnut orchard," *IEEE Trans. Geosci. Remote Sensing*, vol. 29, pp. 852–863, 1991.

[12] K. C. McDonald and F. T. Ulaby, "MIMICS II: Radiative transfer modeling of discontinuous tree canopies at microwave frequencies," in *Proc. IGARSS'90* (College Park, MD), 1990, pp. 20–24.

[13] G. T. Ruck, D. E. Barrick, W. D. Stuart, and C. K. Krichbaum, *Radar Cross-Section Handbook*. New York: Plenum, 1970, pp. 273–274.

[14] K. Sarabandi and T. B. A. Senior, "Low frequency scattering from cylindrical structures at oblique incidence," *IEEE Trans. Geosci. Remote Sensing*, vol. 28, pp. 879–885, 1990.

[15] K. Sarabandi, "Scattering from dielectric structures above impedance surfaces and resistive sheets," *IEEE Trans. Antennas Propagat.*, vol. 40, pp. 67–78, 1992.

$$\bar{\bar{S}}_{TG} = \frac{L}{\pi}\sum_{m=-\infty}^{+\infty}(-1)^m \begin{bmatrix} iC_m^{\mathrm{TM}}R_{||} & \bar{C}_m R_{||} \\ \bar{C}_m R_{\perp} & -iC_m^{TE}R_{\perp} \end{bmatrix} e^{im\phi_s}$$

$$\bar{\bar{S}}_{GT} = \frac{L}{\pi}\sum_{m=-\infty}^{+\infty}(-1)^m \begin{bmatrix} iC_m^{\mathrm{TM}}R_{||} & \bar{C}_m R_{\perp} \\ \bar{C}_m R_{||} & -iC_m^{\mathrm{TE}}R_{\perp} \end{bmatrix} e^{im\phi_s}$$

$$\bar{\bar{S}}_{TTG} = e^{-ik_0 \sin\beta\tilde{\rho}\cos(\phi_s-\tilde{\phi})}\,\frac{(L-\tilde{\rho}\cot\beta)}{\pi} \cdot \sum_{m=-\infty}^{+\infty}(i)^m \begin{bmatrix} i(\Gamma^{\mathrm{TM}}C_m^{\mathrm{TM}}+\bar{\Gamma}\bar{C}_m)R_{||} & (\bar{\Gamma}C_m^{\mathrm{TM}}+\Gamma^{\mathrm{TE}}\bar{C}_m)R_{||} \\ (\Gamma^{\mathrm{TM}}\bar{C}_m+\bar{\Gamma}C_m^{\mathrm{TE}})R_{\perp} & -i(\Gamma^{\mathrm{TE}}C_m^{\mathrm{TE}}+\bar{\Gamma}\bar{C}_m)R_{\perp} \end{bmatrix} \cdot H_m^{(1)}(k_0\sin\beta\tilde{\rho})e^{im(\phi_s-\tilde{\phi})}$$

$$\bar{\bar{S}}_{GTT} = e^{-ik_0 \sin\beta\tilde{\rho}\cos(\phi_s-\tilde{\phi})}\,\frac{(L-\tilde{\rho}\cot\beta)}{\pi} \cdot \sum_{m=-\infty}^{+\infty}(i)^m \begin{bmatrix} i(\Gamma^{\mathrm{TM}}C_m^{\mathrm{TM}}+\bar{\Gamma}\bar{C}_m)R_{||} & (\bar{\Gamma}C_m^{\mathrm{TM}}+\Gamma^{\mathrm{TE}}\bar{C}_m)R_{\perp} \\ (\Gamma^{TM}\bar{C}_m+\bar{\Gamma}C_m^{\mathrm{TE}})R_{||} & -i(\Gamma^{\mathrm{TE}}C_m^{TE}+\bar{\Gamma}\bar{C}_m)R_{\perp} \end{bmatrix} \cdot H_m^{(1)}(k_0\sin\beta\tilde{\rho})e^{im(\phi_s-\tilde{\phi})}$$

$$\bar{\bar{S}}_{TGT} = e^{-ik_0 \sin\beta\tilde{\rho}\cos(\phi_s-\tilde{\phi})}\,\frac{\tilde{\rho}\cot\beta}{\pi} \cdot \sum_{m=-\infty}^{+\infty}(i)^m \begin{bmatrix} i(\Gamma^{\mathrm{TM}}C_m^{\mathrm{TM}}R_{||}+\bar{\Gamma}\bar{C}_m R_{\perp}) & (\bar{\Gamma}C_m^{TM}R_{||}+\Gamma^{\mathrm{TE}}\bar{C}_m R_{\perp}) \\ (\Gamma^{\mathrm{TM}}\bar{C}_m R_{||}+\bar{\Gamma}C_m^{\mathrm{TE}}R_{\perp}) & -i(\Gamma^{\mathrm{TE}}C_m^{\mathrm{TE}}R_{\perp}+\bar{\Gamma}\bar{C}_m R_{||}) \end{bmatrix} \cdot H_m^{(1)}(k_0\sin\beta\tilde{\rho})e^{im(\phi_s-\tilde{\phi})}$$

[16] K. Sarabandi, "Derivation of phase statistics of distributed targets from averaged Mueller matrix," *Radio Sci.*, vol. 27, no. 5, pp. 553–560, Sept.–Oct. 1992.

[17] S. Seker, "Microwave backscattering from a layer of randomly oriented discs with application to scattering from vegetation," *Proc. Inst. Elec. Eng.*, pt. H, *Microwave, Antennas and Propagation*, pp. 497–502, 1986.

[18] L. Tsang and J. Kong, "Application of strong fluctuation random medium theory to scattering from a vegetation-like half space," *IEEE Trans. Geosci. Remote Sensing*, vol. 19, pp. 62–69, 1981.

[19] L. Tsang, M. C. Kubasci, and J. A. Kong, "Radiative transfer theory for active remote sensing of a layer of small ellipsoidal scatterers," *Radio Sci.*, vol. 16, pp. 763–773, 1978.

[20] L. Tsang and J. A. Kong, "Radiative transfer theory for active remote sensing of half-space random media," *Radio Sci.*, vol. 13, pp. 763–773, 1978.

[21] F. T. Ulaby, R,K. Moore, and A. K. Fung, *Microwave Remote Sensing: Active and Pasive*, vol. III, *From Theoy to Applications*. Dedham, MA: Artech House, 1986.

[22] F. T. Ulaby and C. Elachi, *Radar Polarimetry for Geoscience Applications*. Dedham, MA: Artech House, 1990, p. 95.

[23] F. T. Ulaby, K. Sarabandi, K. McDonald, M. Whitt, and M. C. Dobson, "Michigan microwave canopy scattering model (MIMICS)," Univ. Michigan Radiation Laboratory Rep. 022486-3-T, 1988.

[24] F. T. Ulaby, K. Sarabandi, K, McDonald, M. Whitt, and M. C. Dobson, "Michigan microwave canopy scattering model," *Int. J. Remote Sensing*, vol. 11, pp. 1223–1253, 1990.

[25] H. C. Van de Hulst, *Light Scattering by Small Particles*. New York: Wiley, 1957.

Kamal Sarabandi (S'87–M'90–SM'92) was born in Tehran, Iran, on November 4, 1956. He received the B.S. degree in electical engineering from Sharif University of Technology, Tehran, in 1980. From 1980 to 1984 he worked as a microwave engineer in the Telecommunication Research Center in Iran. He entered the graduate program at the University of Michigan in 1984 and received the M.S.E. degree in electrical engineering in 1986 and the M.S. degree in mathematics and the Ph.D. degree in electrical engineering in 1989.

He is currently an Assistant Professor in the Department of Electrical Engineering and Computer Science at the University of Michigan. His research interests include electromagnetic scattering, microwave remote sensing, and the calibaration of polarimetric SAR systems.

Dr. Sarabandi is a member of the Electromagnetics Academy and of USNC/URSI Commission F.

Paul F. Polatin was born in New York City on March 18, 1956. He received the B.A. and M. A. degrees in chemical physics from Columbia University in 1978 and 1979 respectively. From 1978 to 1983 he was involved in varous research projects, including nuclear quadrupole resonance spectroscopy and near-infrared reflectance spectroscopy. From 1984 to 1987 he was with the Upjohn Pharmaceutical Company as a research chemist and laboratory supervisor.

In 1987 he joined the Radiation Laboratory at the University of Michigan. He has since received the M.S.E.E. degree and is currently working to complete the Ph.D. degree in electromagnetic engineering. At present he is engaged in studying the scattering of electromagnetic waves by vegetation media and other problems related to the remote sensing of the terrestrial environment.

Fawwaz T. Ulaby (M'68–SM'74–F'80) received the B.S. degree in physics from the American University of Beirut, Lebanon, in 1964 and the M.S.E.E.. and Ph.D. degrees in electrical engineering from the University of Texas, Austin, in 1966 and 1968, respectively.

Dr. Ulaby is Collegiate Distinguished Professor of Electrical Engineering and Computer Science at the University of Michigan, Ann Arbor, and Director of the NASA Center for Space Terahertz Technology there. His current interests include microwave and millimeter-wave remote sensing, radar systems, and radio

wave propagation. He is the recipient of numerous awards, including the Eta Kappa Nu Association C. Holmes MacDonald Award as "An Outstanding Electrical Engineering Professor in the United States of America for 1975," the IEEE Geoscience and Remote Sensing Distinguished Achievement Award (1983), the IEEE Centennial Medal (1984), the American Society of Photogrammetry's Presidential Citation for Meritorious Service (1984), the Kuwait Prize in Applied Science (1986), the NASA Group Achievement Award (1990), and the University of Michigan Distinguished Faculty Achievement Awared (1991).

Prof. Ulaby served as President of the IEEE Geoscience and Remote Sensing Society (1980–1982), as Executive Editor of its TRANSACTIONS (1983–1985), and as general chairman of several international symposia. He is a member of URSI Commission F and serves on several scientific boards and professional committees.